Maejo International Journal of Energy and Environmental Communication

Journal homepage: https://ph02.tci-thaijo.org/index.php/MIJEEC

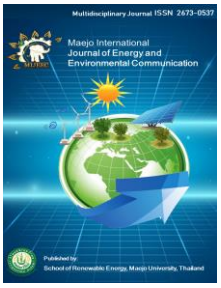

ARTICLE

Optimization and sensitivity analysis of high frequency pulse tube cryocooler for aerospace application

C. Damu[1*], Sumukh S Moudghalya[2], Mrunal M Nerale[2], Rajendra Prasad[3], Upendra Behera[2], Sathyanarayana Reddy[1]

[1]Sambhram Institute of Technology, Bangalore, India
[2]Centre for Cryogenic Technology, Indian Institute of Science, Bangalore, India
[3]Department of Mechanical Engineering, PES University, Bangalore, India.

ARTICLEINFO

Article history:
Received 23 April 2022
Received in revised form
11 May 2022
Accepted 15 May 2022

Keywords:
Computational Fluid Dynamics
Response Surface Methodology
Cryocooler
Heat Transfer

ABSTRACT

The demand for cryogenic cooling systems has been on the rise ever since the development of long-range infrared imaging systems, especially high-frequency Stirling-type cryocoolers which have a vast array of applications in the aerospace sector. While there have been many studies reporting analysis of the pulse tube cryocoolers, these lack an optimization approach with a further sensitivity analysis from computational fluid dynamic (CFD) data to obtain better cold end temperatures. Presently, a response surface method (RSM), has been utilized to characterize the influence of the affecting parameters and a global sensitivity analysis has been conducted to put forward the critical parameters that influence the performance of the device. It is observed that an increase in frequency for lower pressure ratios with higher mean pressure results in better cooling performance in smaller pulse tube diameter models. The sensitivity analysis indicates the operating parameters such as frequency and pressure ratios to be more influential than the geometric parameters with an impact of over 80%.

1. Introduction

The development of pulse tube cryocoolers has been steered by the need for a more efficient, reliable, and vibration-free system in recent times. The pulse tube cryocooler utilizes the surface heat pumping phenomenon to carry heat against the internal temperature gradient hence omitting the inclusion of any moving parts. To further increase the thermal efficiency a long thin tube (inertance tube) which imparts the necessary phase shift for achieving the maximum cooling capacity of the system was introduced by Roach et al. (Roach and Kashani, 1998; Kittel et al., 2004). The theoretical formulation of the complex flow encountered in the Inertance Type Pulse Tube Cryocooler (IPTC), carried out by de Boer et al. (De Boer et al., 2002a) encompasses the effects of the finite reservoir and regenerator volumes through experimental verification. The numerical method is more effective for the simulation of the double inlet pulse tube refrigerator, GM refrigerator, Stirling refrigerator, and other types of refrigerators as reported by Zhu et al. (2004). Implementation of the numerical method using

* Corresponding author.
E-mail address: damu.iisc@gmail.com

Computational Fluid Dynamics (CFD) packages to represent the time-varying temperature and velocity fields in the inertance tube along with the calculation of the heat fluxes at the hot and cold heat exchangers (Flake and Razani, 2004) depicts the progress made in the cryocooler technology. A simple transmission line model of the inertance tube is used to find the maximum phase shift and corresponding optimized dimensions of the inertance tube for different average pressures as outlined in the reports (Radebaugh et al., 2006; Pathak et al., 2012). The effect of ambient temperature and pressure ratios on the phase shift at the inertance tube has an immense impact on the acoustic power and cooling rate of the IPTC as described (Wang et al., 2012). The variation of the pressure and mass flow rates in the corresponding parts of the IPTC is responsible for obtaining the lowest possible cooling as elucidated (Ashwin et al., 2008).

Response surface methodology (RSM) is an approach that can be applied for optimizing mechanical systems (Nariman et al., 2021) through several combinations of factor levels to build a regression model. A 1D analysis of the cryocooler (Panda and Rout et al., 2019) where an optimized COP for a fixed cold end temperature was reported. Even though many researchers have adopted RSM analysis, an optimization method and sensitivity analysis with CFD data for obtaining the lowest cold end temperature is lacking. The present work aims to optimize the expansion device and the operating parameters of frequency and pressure ratio of the cryocooler to find the lowest cold end temperature and respective flow time through RSM. A global sensitivity analysis (Zhang et al., 2015; Cannovo, 2012) is conducted to understand the sensitivity of the design parameters on cooling performance so that further research can be narrowed to those specific variables.

2. Mathematical Formulation

2.1 Governing equations for CFD

The governing equations (ANSYS, 2009a; ANSYS, 2009b) used for the 2 Dimensional (2-D) axisymmetric model are continuity, momentum, and energy equations with considerations towards the dynamic and oscillatory nature of the fluid flow in the IPTC. Extra source terms are added to accommodate the change in porosity across the components of the IPTC.
Equation for conservation of mass:

$$\frac{\partial \rho}{\partial t} + \frac{\partial}{\partial x}(\rho v_x) + \frac{\partial}{\partial r}(\rho v_r) + \frac{\rho v_r}{r} = s_m \qquad 1$$

Equation for conservation of momentum in axial and radial directions:

$$\frac{\partial}{\partial t}(\rho v_x) + \frac{1}{r}\frac{\partial}{\partial x}(r\rho v_x v_x) + \frac{1}{r}\frac{\partial}{\partial r}(r\rho v_r v_x) = -\frac{\partial p}{\partial x} + \frac{1}{r}\frac{\partial}{\partial x}\left[r\mu\left(2\frac{\partial v_x}{\partial x} - \frac{2}{3}\nabla\cdot\vec{v}\right)\right] + \frac{1}{r}\frac{\partial}{\partial r}\left[r\mu\left(\frac{\partial v_x}{\partial r} + \frac{\partial v_r}{\partial x}\right)\right] + F_x \qquad 2a$$

$$\frac{\partial}{\partial t}(\rho v_r) + \frac{1}{r}\frac{\partial}{\partial x}(r\rho v_x v_r) + \frac{1}{r}\frac{\partial}{\partial r}(r\rho v_r v_r) = \frac{\partial p}{\partial r} + \frac{1}{r}\frac{\partial}{\partial x}\left[r\mu\left(\frac{\partial v_r}{\partial x} + \frac{\partial v_x}{\partial x}\right)\right] + \frac{1}{r}\frac{\partial}{\partial r}\left[r\mu\left(2\frac{\partial v_r}{\partial r} - \nabla\cdot\vec{v}\right)\right] - 2\mu\frac{v_r}{r^2} + \frac{2}{3}\frac{\mu}{r}(\nabla\cdot\vec{v}) + \rho\frac{v_z^2}{r} + F_r \qquad 2b$$

where, $\nabla\cdot\vec{v} = (\partial v\_x)/\partial x + (\partial v\_r)/\partial r + v\_r/r$ 2c 2c

The energy equation for porous media:

$$\frac{\partial}{\partial t}\left(\gamma\rho_f E_f + (1-\gamma)\rho_s E_s\right) + \nabla\cdot\left(\vec{v}\left(\rho_f E_f + p\right)\right) = \left[K_{eff}\nabla T - \left(\sum_i h_i J_i\right) + (\bar{\bar{\tau}}\cdot\vec{v})\right] + S_f^h \qquad 3$$

where, $k_{eff} = \gamma k_f + (1-\gamma)K_s$ 3a

2.2 Polynomial Material Equation

To obtain accurate simulation results a polynomial curve for thermal conductivity and specific heat for the temperature range (4K – 300K) is obtained through (NIST, 2010). The 8th-order equations with its coefficients for regenerator material Stainless Steel 304 are illustrated in equations 4a and 4b.

C_p = 22.55020862 - 3.326526689 T^1 + 0.162153947 T^2 - 0.001623541 T^3 + 7.07189E-06 T^4 - 1.20808E-08 T^5 - 2.37935E-12 T^6 + 2.05664E-14 T^7 4a

K = -0.303335492 + 0.114990394 T^1 + 0.000984491 T^2 - 2.69743E-05 T^3 + 2.30832E-07 T^4 - 9.83954E-10 T^5 + 2.11218E-12 T^6 - 1.81863E-15 T^7 4b

2.3 Regression Model

$$y = \beta_0 + \sum_{i=1}^{k} \beta_i x_i + \sum_{i=1}^{k} \beta_{ii} x_i^2 + \Sigma_i \Sigma_j \beta_{ij} x_i x_j + \varepsilon \qquad 5$$

Equation 5 represents a general form of regression equation

(Sarabia et al, 2009). It consists of individual, quadratic, and interaction terms of the input variable along with its respective response. The second-order polynomial equation is selected to be appropriate for the dataset.

3. Methodology

3.1 Modeling and CFD Analysis

A 2-D axisymmetric geometry with all the components of IPTC shown in Figure 1 is constructed according to the dimensions as tabulated in Table 1. A finite element discretization of structured quadrilateral elements is carried out with an element size of 6×10^{-5} m as depicted in Figure 1. To reduce the distance between the wall and the first element, a 5-layer inflation having a growth rate of 1.2 is applied resulting in a first-layer thickness of 1.9×10^{-8} m. A transient approach with a segregated pressure-based solver is adopted for a k-ε turbulent model. Real gas helium is used as the cryogenic fluid. Copper and Steel are the solid materials used in the heat exchangers and nonporous components respectively. Regenerator, CHX, HHX, and Aftercooler are modeled as porous zones by assigning the theoretically calculated inertial and viscous resistances. The applied boundary conditions of the IPTC are attested in Table 1. A User Defined Function (UDF) is developed to generate a sinusoidal pressure waveform and is coupled with the aftercooler thereby eliminating the need for modeling a compressor. A SIMPLE scheme with a PRESTO option for pressure and second-order upwind methods for density and momentum are used. Suitable Under relaxation factors are applied and residual convergence criteria of energy are set at 1×10^{-6} while for continuity, x-velocity, y-velocity, k-ε: 1×10^{-3} is preferred.

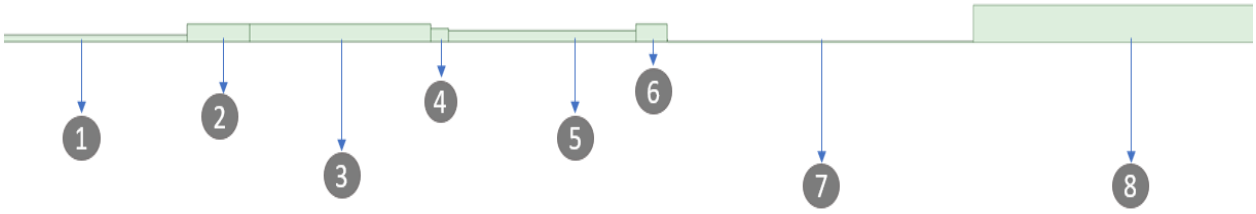

Figure 1 2D Axisymmetric geometry of ITPC.

Table 1 Dimensions and Boundary Conditions of the Model

Sl. No	*Components*	*Radius(m)*	*Length (m)*	*Boundary Condition*
1	Transfer Line	1.55×10^{-03}	1.01×10^{-01}	Adiabatic
2	Aftercooler	4.00×10^{-03}	2.00×10^{-02}	Isothermal (293 K)
3	Regenerator	4.00×10^{-03}	5.80×10^{-02}	Adiabatic
4	Cold end heat exchanger	3.00×10^{-03}	5.70×10^{-03}	Adiabatic
5	Pulse tube	2.50×10^{-03}	6.00×10^{-02}	Adiabatic
6	Hot end heat exchanger	4.00×10^{-03}	1.00×10^{-02}	Isothermal (293 K)
7	Inertance tube	4.25×10^{-04}	6.84×10^{-01}	Adiabatic
8	Reservoir	1.30×10^{-02}	1.30×10^{-01}	Adiabatic

3.2 RSM Analysis

Box-Benhken design is selected to generate higher-order response surfaces to obtain outputs with a minimum number of runs where the values of each factor are equally spaced. Its design levels are arranged in such a way that a rate of increase in design points is directly proportional to the rate of change of the number of polynomial coefficients. For our case of three factors, the

design is constructed as one block with three center points per block containing a two-factor factorial design. A polynomial analysis type is opted for with a maximum process order of six due to the nature of the dataset. To obtain a higher R^2 value and accurate results a quadratic regression model is used. An analysis consisting of 15 runs is conducted with input parameters being pulse tube radius, operating frequency, and pressure ratio for the responses of cold end temperature and flow time as shown in Table 2.

Table 2 Box-Behnken design table

	Factor 1	Factor 2	Factor 3	Response 1	Response 2
Run	**A: pressure Ratio**	**B: Frequency**	**C: Pulse tube radius**	**CHX Temperature**	**Flow Time**
		Hz	Mm	K	s
1	1.5	50	2.5	64	170
2	1.3	75	2.5	58	154
3	1.8	50	2.25	63	165
4	1.3	34	2.5	66	198
5	1.5	34	2.75	63	192
6	1.5	75	2.25	62	160
7	1.8	75	2.5	71	158
8	1.8	50	2.75	64	169
9	1.5	50	2.5	64	173
10	1.5	34	2.25	67	195
11	1.5	75	2.75	68	160
12	1.3	50	2.75	62	176

4. Results and Discussions

The implemented UDF interprets the successive pressurization and depressurization of the working fluid responsible for cooling in IPTC. A temperature contour of the pulse tube cryocooler model with 75Hz frequency, 1.3 pressure ratio, and 2.5mm pulse tube radius which is generated through CFD can be observed in Figure 2a. The cooling in the pulse tube cryocooler is due to the surface heat pumping phenomenon where heat transfer takes place against the temperature gradient in the expansion device as illustrated in Figure 2b. Similarly, a gradient in the density of the working fluid can be observed as shown in Figure 2c which is inversely proportional to temperature throughout space and time of the transient analysis. Fluid flow is confined within the cryocooler omitting any interaction with the external environment, thereby reducing the net mass flow rate to zero as verified by Table 3. This demonstrates the closed-loop system working of the IPTC.

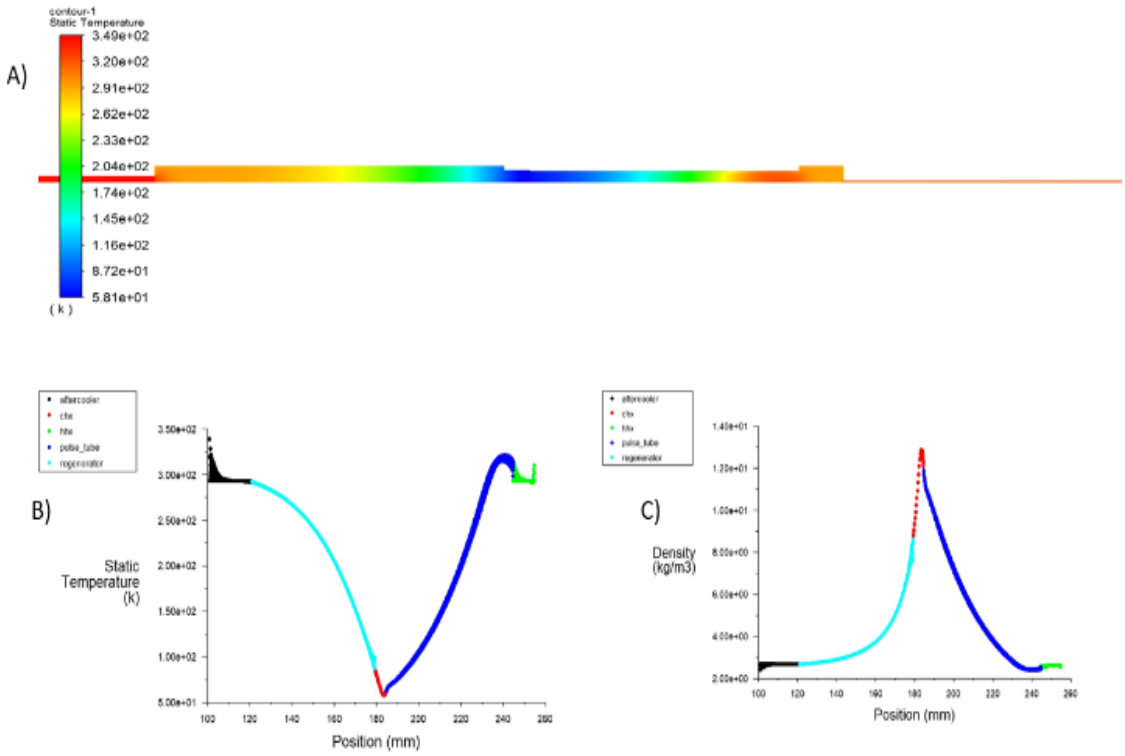

Figure 2 a). Temperature Contour from CFD Analysis.
b) Temperature Gradient throughout the cryocooler.
c) Density Gradient Throughout the Cryocooler

Table 3 Mass Flow Balance in IPTC

Mass Flow Rate	(kg/s)
interior-aftercooler	-0.0028661125
interior-chx	2.5034925e-06
interior-hhx	0.00070907287
interior-inertance tube	0.1180351
interior-pulse tube	-0.00076121028
interior-regenerator	0.00018462245
interior-reservoir	-0.0016103841
interior-transfer line	-0.072318675
aftercooler-surface_body	1.3528207e-05
chx-surface_body.1	-94.9863033e-05
hhx-surface_body.2	0.895104e-05
Inertance_tube-surface_body.3	-0.00057423642
Pulse_tube-surface_body.4	-0.00042212545
regenrator-surface_body.5	5.2183392e-05
reservoir-surface_body.6	-7.4202242e-05
Net	0

4.1 Analysis of Variance

RSM is adopted to analyse the interactive effects of individual parameters (frequency, pressure ratio, pulse tube radius) for the

responses of cold end temperature and flow time. The input parameters are expressed in a form of a regression model where the quality of fit is represented using the R^2 value, P-value and F-value as shown in Table 4 (a and b) and Table 5. The difference between the predicted R^2 value and the adjusted R^2 value is less than 0.2 meaning there is a reasonable agreement between the two for both the responses. Adequate Precision which measures the signal to noise ratio is greater than 4 which is desirable. It indicates an adequate signal and subsequent compatibility of the model to navigate the design space. The Model F-value of 73.27 for CHX Temperature response and 40.55 for flow time response implies the model to be significant. There is only a 0.01% and 0.04% chance respectively for each response to have a F-value this large occur due to noise. P-values less than 0.0500 indicates the model terms to be significant. For the temperature response case A, B, AB, AC, BC, A^2 are significant model terms whereas for the flow time response A, B, B^2 are significant model terms. Values greater than 0.1000 indicate the model terms are not significant. The Lack of Fit F-value of 4.65 implies it is not significant relative to the pure error.

Table 4a Fit Statistics for CHX Temperature

Std. Dev.	0.4751	R^2	0.9925
Mean	64.00	Adjusted R^2	0.9789
C.V. %	0.7424	Predicted R^2	0.8786
		Adeq Precision	32.7141

Table 4b Fit Statistics for Flowtime

Std. Dev.	2.73	R^2	0.9865
Mean	173.73	Adjusted R^2	0.9622
C.V. %	1.57	Predicted R^2	0.8016
		Adeq Precision	18.5743

Table 5 CHX Temperature Quadratic Model

Source	**Sum of Squares**	**df**	**Mean Square**	**F-value**	**p-value**
Model	148.87	9	16.54	73.27	< 0.0001
A-Pressure Ratio	13.28	1	13.28	58.84	0.0006
B-Frequency	7.92	1	7.92	35.06	0.0020
C-Pulse tube radius	1.08	1	1.08	4.79	0.0802
AB	106.18	1	106.18	470.34	< 0.0001
AC	3.59	1	3.59	15.88	0.0105
BC	27.01	1	27.01	119.65	0.0001
A^2	4.79	1	4.79	21.24	0.0058
B^2	0.5501	1	0.5501	2.44	0.1793
C^2	1.38	1	1.38	6.10	0.0566
Residual	1.13	5	0.2258		
Lack of Fit	1.13	3	0.3763		
Pure Error	0.0000	2	0.0000		
Cor Total	150.00	14			

Table 6a Coefficients in Terms of Coded Factors (CHX Temperature)

Factor	Coefficient Estimate	df	Standard Error	95% CI Low	95% CI High	VIF
Intercept	64.29	1	0.2919	63.54	65.04	
A-Pressure Ratio	1.30	1	0.1699	0.8666	1.74	1.04
B-Frequency	1.00	1	0.1696	0.5683	1.44	1.04
C-Pulse tube radius	0.3757	1	0.1716	-0.0656	0.8169	1.04
AB	5.04	1	0.2325	4.44	5.64	1.04
AC	0.9376	1	0.2353	0.3328	1.54	1.02
BC	2.57	1	0.2348	1.96	3.17	1.02
A^2	-1.20	1	0.2599	-1.87	-0.5297	1.03
B^2	0.4100	1	0.2627	-0.2652	1.09	1.03
C^2	0.6107	1	0.2473	-0.0251	1.25	1.01

Table 6b Coefficients in Terms of Coded Factors (Flowtime)

Factor	Coefficient Estimate	df	Standard Error	95% CI Low	95% CI High	VIF
Intercept	166.46	1	1.68	162.15	170.77	
A-Pressure Ratio	-2.52	1	0.9756	-5.02	-0.0091	1.04
B-Frequency	-17.42	1	0.9737	-19.93	-14.92	1.04
C-Pulse tube radius	0.3040	1	0.9855	-2.23	2.84	1.04
AB	3.26	1	1.33	-0.1687	6.69	1.04
AC	1.16	1	1.35	-2.31	4.64	1.02
BC	0.5698	1	1.35	-2.90	4.04	1.02
A^2	-0.3559	1	1.49	-4.19	3.48	1.03
B^2	8.65	1	1.51	4.77	12.52	1.03
C^2	1.15	1	1.42	-2.50	4.81	1.01

The coefficient estimate in Table 6 (a and b) represents the expected change in response per unit change in factor value when all remaining factors are held constant. The intercept in an orthogonal design is the overall average response of all the runs. The coefficients are adjustments around the intercept based on the factor settings. When the factors are orthogonal the Variable Inflation Factors (VIFs) are 1. VIFs greater than 1 indicate multi-collinearity, the higher the VIF the more severe the correlation of factors. As a rough rule, VIFs less than 10 are tolerable. The equation in terms of coded factors as shown in equations 6a for temperature response and 6b for flow time response can be used to make predictions about the responses for given levels of each factor. The coded equation is useful for identifying the relative impact of the factors by comparing the factor coefficients. The final equation in terms of actual factors described in equations 7a and 7b respectively for temperature and flow time, should not be used to determine the relative impact of each factor because the coefficients are scaled to accommodate the units of each factor and the intercept is not at the center of the design space. A graphical representation of the normal probability plots and the distribution of residuals for predicted values is shown in Figure 3 which confirms all the values to be within the prescribed range.

CHX Temperature = 64.29 + 1.30 A + 1.00 B + 0.3757 C + 5.04 AB + 0.9376AC + 2.57 BC – 1.20 A2 +0.41 B2 + 0.61 C2 6a

Flow Time = 166.46 - 2.52 A - 17.42 B + 0.3040 C + 3.26 AB + 1.16 AC + 0.5698 BC - 0.3559 A2 +8.65 B2 +1.15 C2 6b

CHX Temperature = +277.22686 - 26.49537 Pressure Ratio - 2.83525 Frequency - 97.91864 Pulse tube radius + 0.983864

(Pressure Ratio * Frequency) + 15.00205 (Pressure Ratio * Pulse tube radius) + 0.501162 (Frequency * Pulse tube radius) - 19.16667 (Pressure Ratio) ^{2} + 0.000976 (Frequency) ^{2} + 9.77096 (Pulse tube radius) ^{2} 7a

Flow Time = 529.38164 - 73.68117 Pressure Ratio - 4.35726 Frequency - 126.11229 Pulse tube radius + 0.636652 (Pressure Ratio * Frequency) + 18.62756 (Pressure Ratio * Pulse tube radius) + 0.111172 (Frequency * Pulse tube radius) - 5.69444 (pressure Ratio) ^{2} + 0.020574 (Frequency) ^{2} + 18.47931 (Pulse tube radius) ^{2} 7b

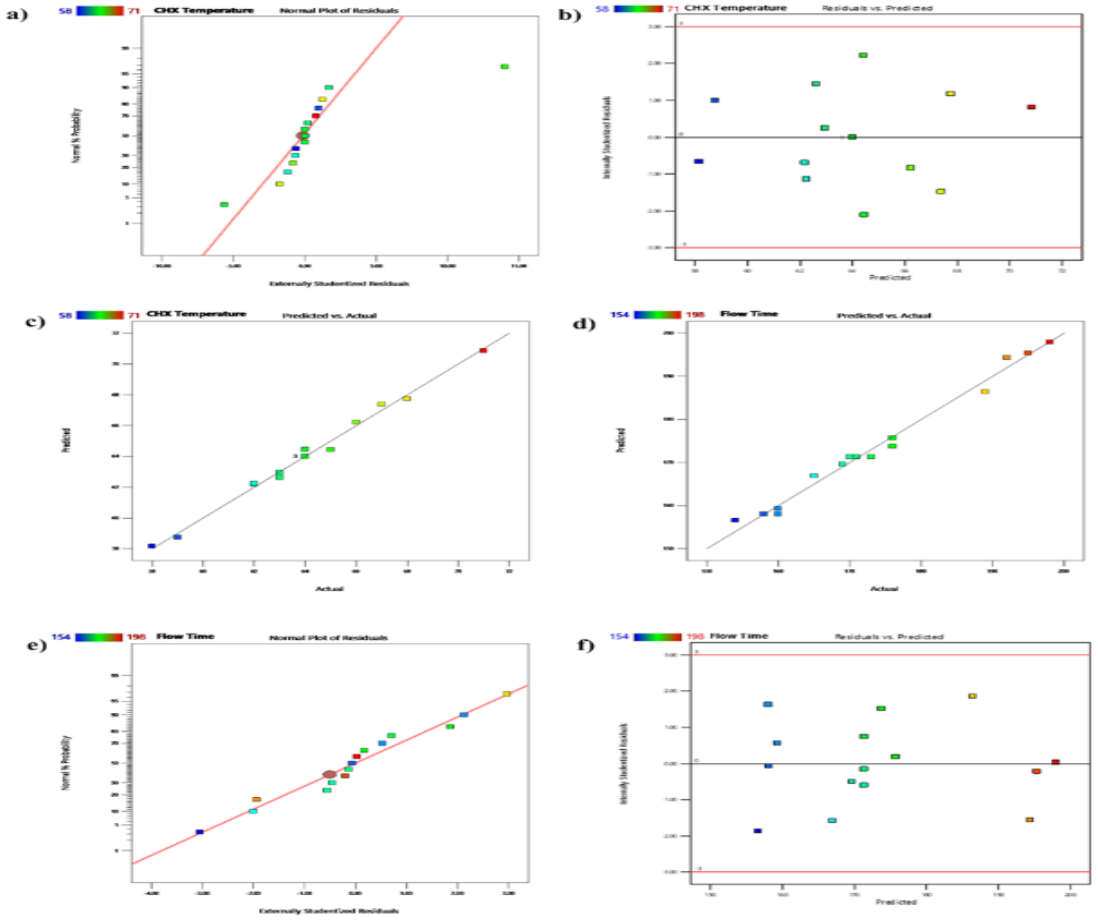

Figure 3 a) & e) Residual Plots for CHX Temperature and Flow Time
b) & f) Residuals vs Predicted limits for CHX Temperature and Flow Time
c) & d) Predicted vs Actual Graph for CHX Temperature and Flow Time

4.2 Optimization and Sensitivity Analysis

From the analysis conducted, an improved cold end temperature is observed for higher frequency and lower pressure ratios having high mean pressure as shown in Figure 4a. This is because the inertance effect which is responsible for the phase shifting mechanism is more responsive in this state. It is also observed that for higher pressure ratios with a low mean pressure, lower frequency is preferred thus creating a bell-shaped response surface. Figure 4b shows the impact of frequency with respect to pulse tube radius on cold end temperature. For lower frequencies a bigger radius is proven to give better cooling due to lower levels of shear stress acting radially in the pulse tube. In the case of higher frequencies better performance is observed for pulse tubes of smaller radius. The effect of pressure ratio and pulse tube radius is such that lower ratios in general have better no-load cooling for the range of pulse tube radii as illustrated in Figure 4b. With respect to flow time in order to reach temperature saturation, frequency is the most significant parameter as flow time reduced with increase in frequency as shown in Figure 4c which is desirable. The coded

equation 6a from the optimization model is used to conduct the sensitivity analysis of all the factors used in the analysis. Operating parameters are more sensitive to cooling performance than the dimensional parameters with frequency being the most sensitive followed by pressure ratio as described in Figure 5. Thus, a minute change in operating parameters will have a drastic effect on performance.

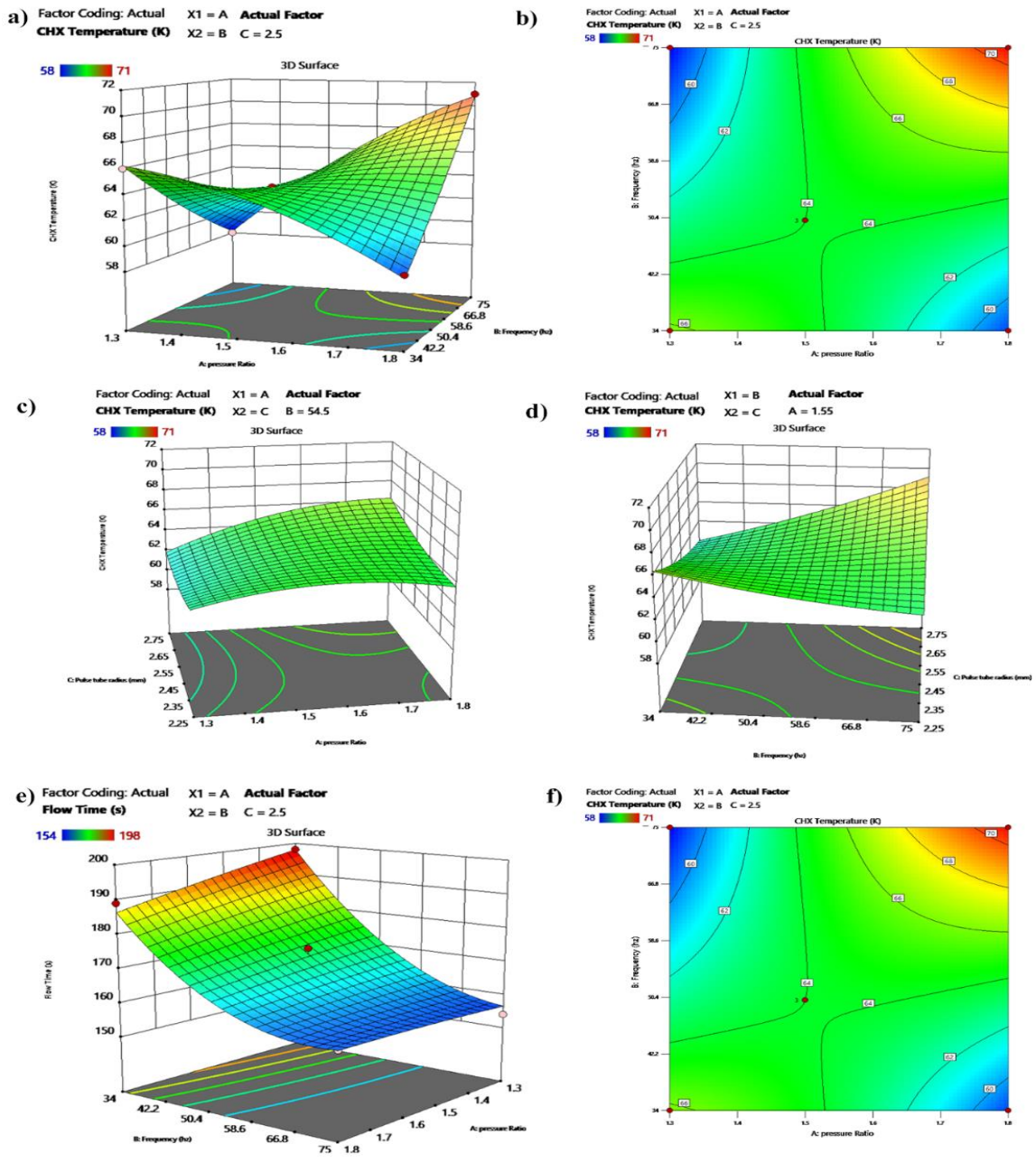

Figure 4 a & b) CHX Temperature Response w.r.t. Frequency and Pressure Ratio
c) CHX Temperature Response w.r.t. Pressure Ratio and Pulse Tube Radius
d) CHX Temperature Response w.r.t Frequency and Pulse Tube Radius
e & f) Flow Time Response w.r.t Frequency and Pressure Ratio

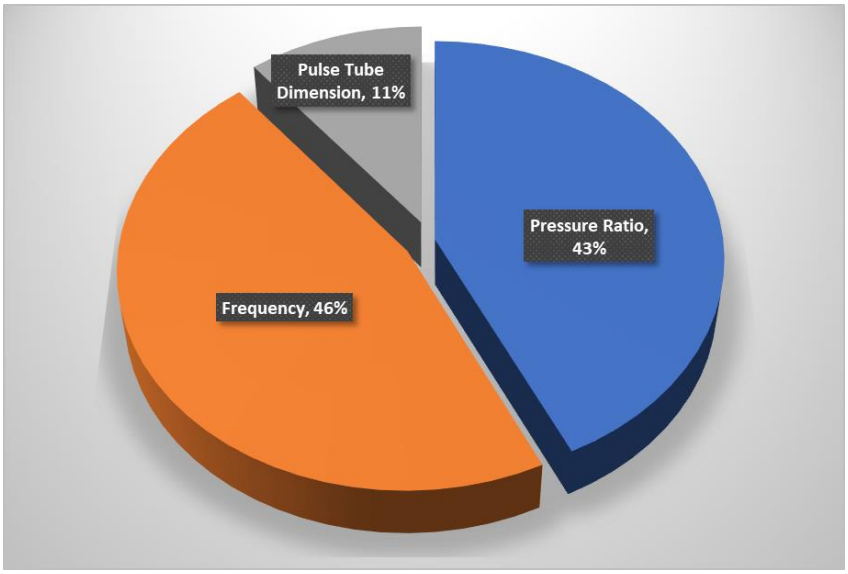

Figure 5 Sensitivity Chart of Parameters Affecting CHX Temperature.

5. Conclusion

The present study focuses on optimization of the significant parameters of a pulse tube cryocooler. To achieve this, multiple cases of CFD studies are conducted and a design table is drafted for RSM Optimization. From the RSM coded equation, a global sensitivity analysis is carried out to find the significant parameters for cooling performance. The following deductions are formulated from the analysis:

- For compressors with lower pressure ratios (1.3 – 1.5) having a high mean pressure, a higher frequency will yield better performance whereas for a higher-pressure ratio with low mean pressure, lower frequency is preferred.
- In order to reduce the radius of the pulse tube, the cryocooler must be operated at a higher frequency with a high mean pressure to maintain the cooling performance.
- From the sensitivity analysis, it is observed that operating parameters like frequency and pressure ratio are more vital when compared with dimensional parameters to increase the performance of the cryocooler.

Nomenclature

ρ – Density, kg m^{-3}

t – Time, s

v_x – Velocity in x-direction, m s^{-1}

v_r – Velocity in r-direction, m s^{-1}

s_m – Source Term

p – Pressure, Kg m^{-1}

μ – Molecular Viscosity, Kg m^{-1} s^{-1}

$\vec{v}$ – Velocity Vector, m s^{-1}

F_x – Axial Force, Kg m s^{-2}

F_r – Radial Force, Kg m s^{-2}

γ - Porosity

ρ_f – Fluid Density, kg m^{-3}

E_f – Total Fluid Energy, Kg m^2 s^{-2}

ρ_s – Solid Density, kg m^{-3}

E_s – Total Solid Medium Energy, Kg m^2 s^{-2}

$\bar{\bar{\tau}}$ – Stress Tensor, N m^{-2}

S_f^h - Fluid Enthalpy Source Term

k_{eff} - Effective Thermal Conductivity of the Medium, W m^{-1} K^{-1}

T – Temperature, K

C_p – Specific Heat, J Kg^{-1} K^{-1}

K – Thermal Conductivity, W m^{-1} K^{-1}

y – Response Function

β_i – Linear Term Coefficient

β_{ii} – Quadratic Term Coefficient

β_{ij} – Interaction Term Coefficient

x_i & x_j - Independent Terms

References

Ahmad, N. O. O. R. A. Z. I. A. H., & Janahiraman, T. V. 2014. A study on regression model using response surface methodology. Applied Mechanics and Materials, 666, 235-239.

ANYS 2009a. https://www.afs.enea.it/project/neptunius/docs/fluent/html/th/node11.htm. Accessed on 27th Sept 2022

ANYS 2009b. https://www.afs.enea.it/project/neptunius/docs/fluent/html/ug/node233.htm. Accessed on 27th Sept 2022

Ashwin, T.R, Narasimham, G.S.V.L. & Jacob, S. 2008. Numerical modeling of inertance tube pulse tube refrigerator. In Proceedings of ICHMT International Symposium on Advances in Computational Heat Transfer. Begel House Inc.

Cannavó, F. 2012. Sensitivity analysis for volcanic source modeling quality assessment and model selection. Computers & geosciences, 44, 52-59.

de Boer, P.C.T. 2002b. Maximum attainable performance of pulse tube refrigerators. Cryogenics 42 (2002) 123–125.

De Boer. P.C.T. 2002a. Performance of the inertance pulse tube. Cryogenics. 42: 209-221

De Boer. P.C.T. 2011. Optimal performance of regenerative cryocoolers. Cryogenics 51, 105–113.

Flake. B & Razani A. 2004. Modeling pulse tube cryocoolers with CFD. American Institute of Physics, Conference Proceedings, 710: 1493-1499.

Kittel, P., Feller, J., Roach, P., Kashani, Ali., & Helvensteijn, B. 2004. Cryocoolers for Space. International Thermal Detectors Workshop

Nariman, N. A., Hamdia, K., Ramadan, A. M., & Sadaghian, H. 2021. Optimum Design of Flexural Strength and Stiffness for Reinforced Concrete Beams Using Machine Learning. Applied Sciences, 11(18), 8762.

NIST,2010.https://trc.nist.gov/cryogenics/materials/304Stainless/304Stainless_rev.htm. Accessed on 27th Sept 2022.

Panda, D., & Rout, S. K. 2019. Optimization of an inertance pulse tube refrigerator using the particle swarm optimization algorithm. Heat Transfer—Asian Research, 48(8), 3508-3537.

Pathak, M.G., Ghiaasiaan, S.M., Radebaugh, R., Kashani, A., & Feller. J. 2012. The Design and Development of a High-Capacity Cryocooler Regenerator for Exploration. AIAA SPACE Conference & Exposition 2012.

Radebaugh, R., Lewis, M., Luo, E., Pfotenhauer, J. M., Nellis., G. F., & Schunk. L. A. 2006. Inertance tube optimization for pulse tube refrigerators. Advances in Cryogenic Engineering: Transactions of the Cryogenic Engineering Conference – CEC, Vol. 51, American Institute of Physics.

Roach, P. R., & Kashani, A. 1998. Pulse tube coolers with an inertance tube: theory, modeling, and practice. In Advances in cryogenic engineering (pp. 1895-1902). Springer, Boston, MA.

Sarabia, L. A., Ortiz, M. C., & Sánchez, M. S. 2020. Response surface methodology. https://doi.org/10.1016/B978-044452701-1.00083-1.

Wang, B., Wang, L.Y., Zhu, J.K., Chen, J., Li, Z.P., Gan, Z.H., Qiu, L.M. 2012. Cryocoolers 17, International Cryocooler Conference Inc.

Zhang, X. Y., Trame, M. N., Lesko, L. J., & Schmidt, S. 2015. Sobol sensitivity analysis: a tool to guide the development and evaluation of systems pharmacology models. CPT: pharmacometrics & systems pharmacology, 4(2), 69-79.

Zhu, S. & Matsubara, Y. 2004. Numerical method of inertance tube pulse tube refrigerator. Cryogenics, 44: 649-660.